J Comp Physiol A (2003) 189: 1–17
DOI 10.1007/s00359-002-0370-2

ORIGINAL PAPER

D.G. Stavenga

Angular and spectral sensitivity of fly photoreceptors. I. Integrated facet lens and rhabdomere optics

Received: 17 July 2002 / Revised: 4 October 2002 / Accepted: 5 October 2002 / Published online: 10 December 2002

Abstract Three optical components of a fly's eye determine the angular sensitivity of the photoreceptors: the light diffracting facet lens, the wave-guiding rhabdomere and the light-absorbing visual pigment in the rhabdomere. How the integrated optical system of the fly eye shapes the angular sensitivity curves is quantitatively analyzed in five steps: (1) scalar diffraction theory for low Fresnel-number lenses is applied to four different facet lenses, with diameter 10, 20, 40, and 80 μm, respectively, assuming a constant F-number of 2.2; (2) optical waveguide theory is used to calculate waveguide modes propagating in circular cylindrical rhabdomeres with diameter 1.0, 2.0, and 4.0 μm, respectively; (3) the excitation of waveguide modes is studied with the tip of the waveguide positioned in the focal plane as well as outside this plane; (4) the light absorption from the various propagated modes by the visual pigment in the rhabdomere is calculated as a function of the angle of the incident light wave; and (5) the angular sensitivity of the photoreceptor is obtained by normalizing the total light absorption. Four wavelengths are considered: 300, 400, 500 and 600 nm. The analysis shows that the wavelength dependency of the lens diffraction is strongly compensated by that of the waveguide modes, an effect which is further enhanced by the decrease in light absorption when the mode number increases. The angular sensitivity of fly photoreceptors is robust to defocus and largely wavelength independent for all except very slender rhabdomeres.

Keywords Facet lens · Rhabdomere · Spatial acuity · Visual pigment · Waveguide modes

D.G. Stavenga
Department of Neurobiophysics,
University of Groningen,
9747 AG Groningen, The Netherlands
E-mail: stavenga@phys.rug.nl

Introduction

Animal eyes sample optical information from the environment with their photoreceptor array. The photoreceptors of compound eyes are organized in small units, the ommatidia, recognizable in the intact eye by the facets. The facet lens focuses light into the photoreceptors, and the surrounding screening pigment cells protect the photoreceptors from off-axis and stray light. The photoreceptors capture light with their visual pigment molecules, which are concentrated in slender, cylindrical structures, the rhabdomeres. In fly eyes, the rhabdomeres of the individual photoreceptors are spatially separate, each functioning as a single optical waveguide (reviewed by Hardie 1985). The tip of the rhabdomere more or less coincides with the focal plane of the facet lens. Due to its small cross-section, incident light is channeled into the rhabdomere from a narrow range of directions, giving the photoreceptors limited fields of view. The field is given by the spatial distribution function, called the angular sensitivity (van Hateren 1984). The angular sensitivity often approximates a Gaussian function (Götz 1964; Warrant and McIntyre 1993); its symmetry axis, marking the direction of maximal sensitivity of the photoreceptor, is called the visual axis. The lattice of the visual axes together with the angular sensitivity of the individual photoreceptors determines the spatial acuity of the eye.

Understanding an animal's visual behavior inevitably requires knowledge of the optical performance of the eyes, and therefore the optical factors determining spatial acuity and angular sensitivity take the center stage in discussions of eye design (see, for example, Warrant and McIntyre 1993; Land and Nilsson 2002). Facet lenses are small, and therefore diffraction is thought to be the principal limit to the spatial acuity of insect eyes. The other limitation is the width of the rhabdomere (or that of the fused rhabdom, in apposition eyes). To combine these two factors, Snyder (1979) introduced a heuristic, simple formula, which has become widely applied,

although it is fundamentally incorrect, as it was derived from partly geometric optical arguments (van Hateren 1984; Warrant and McIntyre 1993; Land and Nilsson 2002), and, more importantly, it neglects the waveguide properties of the light-absorbing rhabdomeres. These can distinctly modify the angular sensitivity (Pask and Barrell 1980a, 1980b).

The angular sensitivity of a photoreceptor is measured experimentally by varying the angular position of a point light source. The light intensity necessary to elicit a criterion response is then assessed, and subsequently the photoreceptor's angular light sensitivity is normalized to its maximal value, yielding the angular sensitivity function. The angular sensitivity more or less varies with the light source's wavelength (Horridge et al. 1976; Smakman et al. 1984), but this detail is often implicitly neglected (e.g., Burton et al. 2001). Another important characteristic of a photoreceptor is its spectral sensitivity. This function is measured experimentally in a similar way, by varying the wavelength of the light source and then determining a criterion intensity, with subsequent normalization to the sensitivity value at the peak wavelength, λ_{max}. The possible dependence of the spectral sensitivity on the spatial extent of the light source is also usually neglected. The consequence of normalization is of course that the absolute light sensitivity, in fact the central characteristic of a photoreceptor, is no longer recognizable.

Light sensitivity of a fly photoreceptor cell firstly depends on the efficiency of channeling light by the facet lens into the rhabdomere, which depends on the angle of light incidence and wavelength, but also on other additional and equally important factors such as the efficiency of light capture by the visual pigment molecules and the conversion of the absorbed light energy into a visual signal. We have to realize that light sensitivity depends in a complex way on the angle of incidence of the stimulating light and its spectral content. We therefore have to critically assess to what extent angular and spectral sensitivity are separable.

Barrell and Pask (1979) developed the first proper treatment of the integrated facet lens-rhabdomere system, which was subsequently extended by van Hateren (1984). This theory allowed a quantitative analysis of electrophysiological (Smakman et al. 1984) as well as optical (van Hateren 1984) measurements of the angular sensitivity of fly photoreceptors. The experimental results could be satisfactorily described by model calculations treating an ideal lens with the tip of an optical waveguide in its focal plane (Smakman et al. 1984; van Hateren 1984). A critical point of the theoretical treatment of Barrell and Pask (1979) is that it is based on classical diffraction theory (Born and Wolf 1975). This approach is possibly not fully adequate, because light focusing by small lenses starts to deviate from the classical case (Kuiper 1965; Li and Wolf 1984). Direct optical measurements on the diffraction patterns of isolated blowfly facet lenses indeed showed that classical diffraction optics fails in this case (Stavenga and van Hateren 1991), necessitating a revision of the theoretical analysis of photoreceptor angular sensitivity developed by Barrell and Pask (1979).

The aim of this paper is to investigate how the components of the integrated optical system of fly eyes - the facet lens, the rhabdomere, and the visual pigment- shape the photoreceptors' angular sensitivity function for light of different wavelengths. The steps taken in the present analysis are as follows. I first consider monochromatic point sources illuminating a fly facet lens, leading to an expression for the resulting light distribution in image space. The strong wavelength dependence of the light patterns is illustrated by a few examples. In the following step, I recall the optical waveguide theory applicable to a fly rhabdomere and give examples of the waveguide modes that can propagate in a rhabdomere. I subsequently treat the integrated optical system of the combination facet lens-rhabdomere to obtain formulae for the angular excitation function for modes of a rhabdomere. The derived expressions are then used to calculate the amount of light excited and propagated in the various modes. It thus appears that mode excitation is rather robust to slight longitudinal variations in the position of the rhabdomere tip, be it distally or proximally from the focal plane. In the next step, I calculate the degree of light absorption from the modes by the visual pigment as a function of light wavelength and angle of incidence. Finally, I deduce angular sensitivities for a number of lens and rhabdomere sizes. It appears, almost surprisingly, that diffraction effects can be largely neglected and that rhabdomere size is the determining factor for the angular sensitivity of fly photoreceptors.

Anatomy and optical characteristics of an ommatidium of a fly eye

The anatomy of the ommatidia of a fly eye is schematically shown in Fig. 1a, b. Beneath the corneal facet lens exists a transparent pseudocone. The ommatidium is enveloped by pigment cells. Semper cells form an interface between pseudocone and photoreceptor cells. The rhabdomeres of the six large photoreceptors, R1–6, run along the full length of the cell body, with range 220–340 μm in the blowfly *Calliphora vicina*. The same distance is shared by the rhabdomeres of the R7 and R8 photoreceptors, with R7 taking the distal 60% and R8 the proximal 40% part (Hardie 1985).

The facet lens and the rhabdomere together determine the angular sensitivity of a photoreceptor. Diffraction by the facet lens depends on the light wavelength, the facet lens diameter and its focal distance. The wavelengths relevant for fly photoreceptors range from ca. 300 nm to above 600 nm. The diameter of facet lenses in the male blowfly *Calliphora* ranges from 20 μm to 40 μm, but in the male *Chrysomia* values up to 80 μm are reached (Stavenga et al. 1990; van Hateren et al. 1989). Detailed optical measurements show that the F-number, i.e., the ratio of the focal

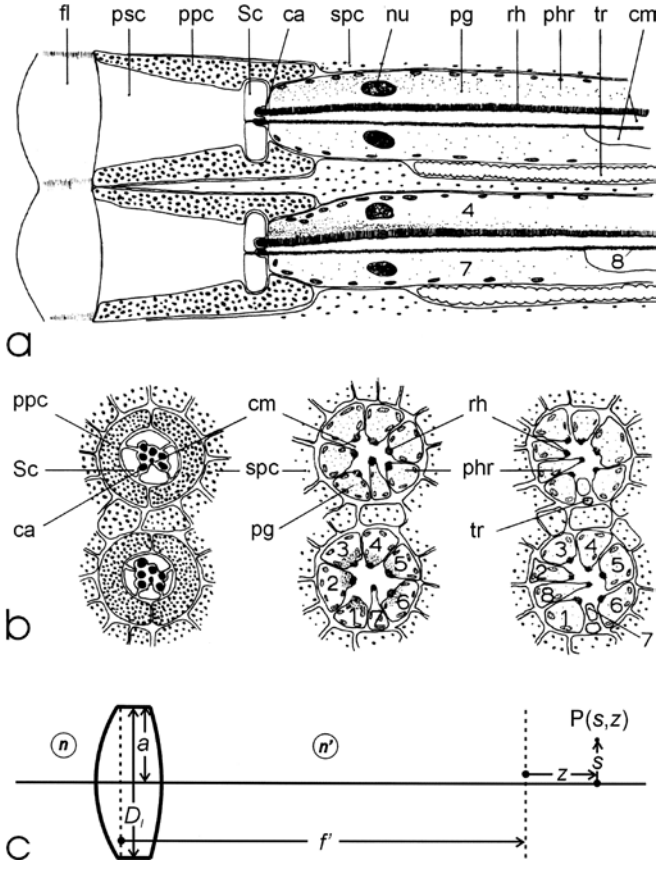

Fig. 1 Optics of fly ommatidia; longitudinal (**a**) and cross-sections (**b**). A fly ommatidium consists of a facet lens (*fl*), a pseudocone (*psc*), primary pigment cells (*ppc*), secondary pigment cells (*spc*), Semper cells (*Sc*), a trachea (*tr*); the photoreceptors cells (*phr*), with nucleus (*nu*), have rhabdomeres (*rh*), topped by caps (*ca*) and in their middle a central matrix (*cm*). The photoreceptor cells contain pigment granules (*pg*), which in the dark-adapted situation are held back from the rhabdomere region (upper ommatidia), but upon light adaptation are driven towards the rhabdomere boundary region (lower ommatidia). The cross-sections of **b** are at the level of the caps, in the distal region, and in the proximal region of the retina, respectively (from left to right). **c** Diagram of the optics of a fly facet lens with radius a, diameter D_l, and image focal distance f'. The diffraction field due to a light point source at infinity in a point P(s, z) is considered; s is the distance of P to the axis, and z is the distance to the image focal plane. The refractive indices of object and image space are n and n', respectively (modified from Stavenga 1975)

distance and the facet diameter, remains rather constant over this wide range of diameters: $F = 2.0 \pm 0.2$ (Stavenga et al. 1990). Model calculations on mode radiation patterns and electrophysiological measurement of the Stiles-Crawford effect in *Calliphora* yielded F-numbers ranging from 2.0 to 2.5 in the ventral and lateral eye regions, but up to 3 for the dorsal area (van Hateren 1985). Measurements of interommatidial angles in a male housefly *Musca* yielded a value of $F = 1.9$ for facet lenses with diameter between 17 μm and 23 μm (Stavenga 1975). For the fruitfly *Drosophila*, where the facet lens diameter is about 16 μm, a focal distance of 20 μm was derived (Franceschini and Kirschfeld 1971), yielding a very low F-number of 1.25. It therefore seems that the F-number is not the same for different fly species, but to keep the present analysis manageable a constant value of $F = 2.2$ is assumed in the model calculations.

The diameter of the rhabdomere and the refractive indices of the media within and surrounding it determine the waveguide properties of the rhabdomere. The diameter of the very slender central rhabdomeres of housefly R7 and R8 photoreceptors is about 0.6–1.0 μm (Hardie 1985), and that of the peripheral rhabdomeres R1–6 is distally 1.5–2.0 μm (Smakman et al. 1984; Hardie 1985). The latter rhabdomeres taper proximally to a diameter of ca. 1.0 μm (Boschek 1971). An extreme example is the male blowfly *Chrysomia* with strongly tapering R1–6 rhabdomeres having a distal diameter of well over 4 μm (van Hateren et al. 1989). For the refractive index of the rhabdomere medium a value of 1.363 may be assumed (Stavenga 1974; Beersma et al. 1982). The refractive index very slightly varies with wavelength, due to anomalous dispersion, but the effects on the waveguide properties are negligible (Stavenga and van Barneveld 1975). A value of 1.340 is assumed for the refractive index of the surrounding medium (Seitz 1968). At the distal end of the rhabdomeres, a cylindrical, extracellular cap exists (Seitz 1968), possibly serving as a mechanical support (Pask and Barrell 1980b). The photoreceptor cells contain small pigment granules, which accumulate near the rhabdomere upon light adaptation. The light absorbing granules affect the propagated waveguide modes and thereby the angular sensitivity (Smakman et al. 1984).

Diffraction optics of a small lens

Light focusing by a fly facet lens is described by the scalar diffraction theory for high power, low-Fresnel-number lenses developed by Li and Wolf (1984). The case of a monochromatic light wave emitted by a distant point source and focused by the facet lens is equivalent to that of a circular aperture of radius a in an opaque screen with a uniform, spherical wave, converging at the image focal point (Fig. 1c). The aperture plane corresponds to the image principal plane of the facet lens, with image focal length $f' = n'f$, where n' is the refractive index of image space and f the object focal length (the refractive index of object space is taken to equal that of free space: $n = 1$; primed optical parameters refer to image space, the corresponding quantities of object space are then without a prime). The amplitude of the light wave in the spherical wave front is (Li and Wolf 1984):

$$Q_a = A\frac{e^{-ik'f'}}{f'} \tag{1}$$

where wavenumber $k' = 2\pi n'/\lambda = 2\pi/\lambda'$; λ and λ' are the light wavelengths in free and image space, respectively. The light intensity, i.e., the light power density, is

the modulus of the amplitude squared:

$$I_a = |Q_a|^2 = \left(\frac{|A|}{f'}\right)^2 \tag{2}$$

and the total light power is:

$$P_a = \pi a^2 I_a = \pi\left(\frac{a|A|}{f'}\right)^2 = \pi q'^2 |A|^2 \tag{3}$$

where

$$q' = \frac{a}{f'} \tag{4}$$

In the following I assume that a unit power of monochromatic light passes the aperture, i.e., $P_a = 1$ W. Then:

$$|A| = \frac{1}{q'\sqrt{\pi}} \tag{5}$$

The diffracted field in a point P = P(s,z) near the focal point, located at (radial) distance s from the lens symmetry axis and at (longitudinal) distance z from the focal plane (Fig. 1c), is given by (Born and Wolf 1975, p. 437; Li and Wolf 1984):

$$Q(s,z) = Be^{i\Phi}\int_0^1 J_0(v\rho)e^{-i\frac{u\rho^2}{2}}\rho d\rho \tag{6}$$

where

$$u = \frac{k'}{\delta}q'^2 z,\ v = \frac{k'}{\delta}q' s,\ B = -i\frac{k'}{\delta}q'^2 A, \text{ and } \Phi = k'\left(z + \frac{s^2}{2\delta f'}\right) \tag{7a - d}$$

$$\delta = \frac{f' + z}{f'} = 1 + \frac{z}{f'} \tag{7e}$$

The light intensity in P is given by:

$$I(s,z) = |Q(s,z)|^2 \tag{8}$$

The light distribution in the focal plane ($z = 0$) is described by the well-known Airy-diffraction formula:

$$I(s,0) = |Q(s,0)|^2 = I_0\left[\frac{2J_1(v)}{v}\right]^2 \tag{9}$$

where I_0, the intensity in the focal point, is:

$$I(0,0) = I_0 = \left(\frac{\pi q'^2 |A|}{\lambda'}\right)^2 \tag{10}$$

Assuming unit total light power, it follows (with Eq. 5) that:

$$I_0 = \frac{\pi a^2}{(\lambda' f')^2} = \frac{\pi a^2}{(\lambda f)^2} = \frac{\pi}{4}\frac{1}{\lambda^2 F^2} \tag{11}$$

where F is the F-number of the lens:

$$F = \frac{f}{D_l} \tag{12}$$

and $D_l = 2a$ is the lens diameter (Fig. 1c). Equation 11 shows that the intensity in the focal point is inversely proportional to the square of the wavelength.

Li and Wolf (1984) have demonstrated that the Fresnel number:

$$N = \frac{a^2}{\lambda f} = \frac{D_l F}{4\lambda} \tag{13}$$

is an important parameter determining the diffraction pattern of small lenses. When the Fresnel number is large, as is generally the case for normal lenses, $\Phi = k'z$ and $\delta = 1$ (Eq. 7). The light intensity distribution then becomes symmetrical with respect to the focal point (Born and Wolf 1975). This classical situation no longer holds when $N < 10$ (Li and Wolf 1984), values attained by the small facet lenses of flies (Stavenga and van Hateren 1991).

Figure 2 presents the intensity distribution due to diffraction of a light wave that enters a facet lens (diameter $D_l = 20$ μm) parallel to its axis. Five planes perpendicular to the axis are considered, at $z = -10$, –5, 0, 5, and 10 μm, and four light wavelengths: $\lambda = 300$, 400, 500, and 600 nm, respectively. The curves in Fig. 2c ($z = 0$ μm) are described by the Airy formula (Eq. 9). The peak amplitude is inversely proportional to the

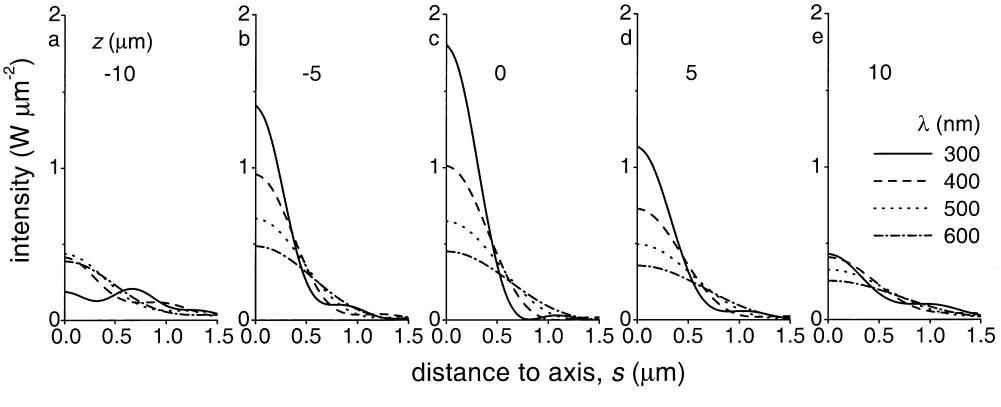

Fig. 2 Intensity distribution for a facet lens with diameter $D_l = 20$ μm and F-number $F = 2.2$ as a function of the transversal distance to the axis, s, in five planes located at $z = -10$ (**a**), –5 (**b**), 0 (**c**), 5 (**d**), and 10 μm (**e**) from the image focal plane, for four wavelengths: 300, 400, 500, and 600 nm. The intensity in the focal point (**c**) is inversely proportional to the wavelength squared. The total incident light power in all cases is 1 W

square of the wavelength (Eq. 11) and the intensity rapidly falls off when the distance to the axis increases.

Figure 3 gives the axial intensity distribution, i.e., as a function of z, the distance to the image focal plane, for four lenses with diameter D_l = 10, 20, 40, and 80 μm, respectively. The intensity distributions are for all four wavelengths rather similar for the different lens sizes, but the distributions are asymmetric, especially for smaller lenses and longer wavelengths. Only for the large lens (80 μm), is the light distribution virtually symmetrical around the focal point (z = 0 μm) for all wavelengths.

A comparison of Figs. 2 and 3 shows that the intensity distribution depends much more strongly on the transversal distance, s, than on the longitudinal distance, z; the halfwidths are about 1 μm and 15 μm, respectively, depending somewhat on the wavelength. The 3-D intensity distributions in Fig. 4, presenting the case of a lens with diameter D_l = 20 μm, dramatically visualize the longitudinal stretch of the diffraction pattern, as well as the extreme dependence of the distributions on the wavelength. As we will see later on, the severe dependence of the facet lens imaging on light wavelength is almost fully annihilated by the equally severe wavelength dependence of the waveguide properties of the rhabdomere (see also van Hateren 1989).

Optical waveguide modes

Light propagation in a fly rhabdomere is described by optical waveguide theory (Snyder and Love 1983). Light

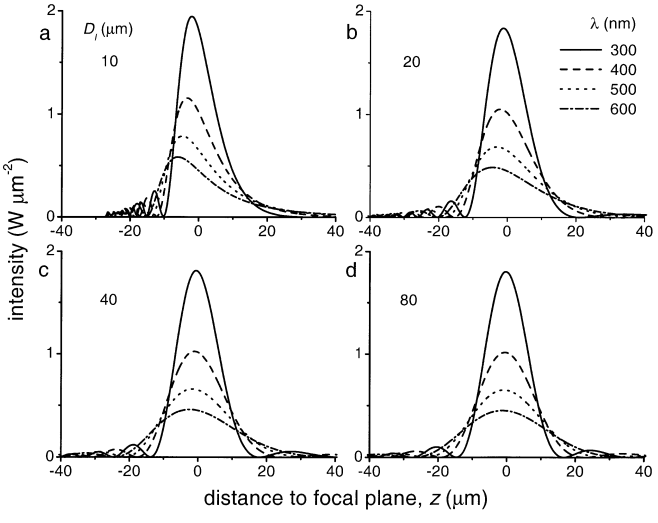

Fig. 3 Intensity distribution at the lens axis due to diffraction for three lenses with diameter D_l = 10 (**a**), 20 (**b**), 40 (**c**), and 80 μm (**d**), respectively, as a function of the longitudinal distance to the image focal plane, z, for four wavelengths: 300, 400, 500, and 600 nm. The intensity distributions strongly depend on wavelength, but are rather similar for one and the same wavelength for all lens sizes, because of the constant F-number: F = 2.2. The axial light distribution becomes progressively asymmetric for smaller lenses and longer wavelengths. The shift of the intensity maximum (the focal shift) is towards the lens, in the distal direction. The total incident light power is 1 W

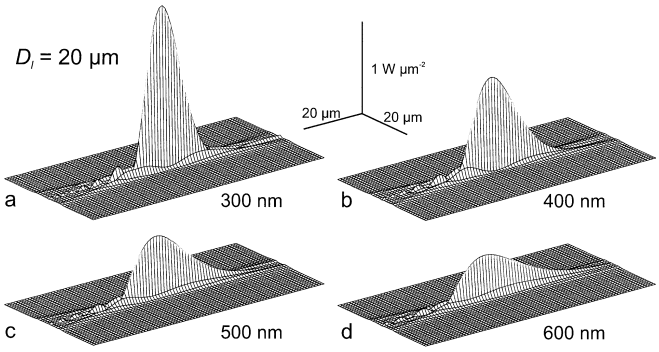

Fig. 4 3-D distribution of the diffraction patterns for a facet lens with diameter D_l = 20 μm. The intensity in the focal point is extreme for short wavelengths, because both the transversal and the lateral spread are smallest there (see Figs. 2 and 3, respectively). The ground planes span a longitudinal range of $-80 < z < 80$ μm and a transversal range of $-20 < s < 20$ μm. The total incident light power is 1 W

is propagated along a slender dielectric cylinder in fixed patterns, so-called modes, which are determined by the light wavelength λ, the rhabdomere diameter D_r, and the refractive indices of the media inside and outside the waveguide, n_1 and n_2, respectively (Fig. 5). When the difference between the refractive indices, n_1-n_2, is small, a set of simple orthonormal linearly polarized modes can be derived (Gloge 1971; Yariv 1985). When the field incident at the waveguide is polarized along the x-axis (Fig. 5), the field of a (bound) waveguide mode, with index p, is given by (Barrell and Pask 1979; see Yariv 1985):

$$e_p(R,\varphi) = \frac{M_p(R)}{\sqrt{N_p}}\cos(l\varphi) \tag{14}$$

with

$$M_p(R) = J_l(UR), \quad R \le 1, \tag{15a}$$

$$M_p(R) = \frac{J_l(U)}{K_l(W)}K_l(WR), \quad R \ge 1 \tag{15b}$$

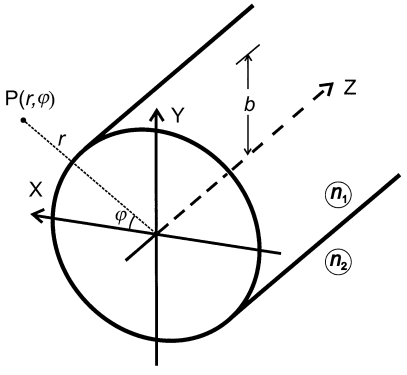

Fig. 5 Diagram of the distal end of a fly rhabdomere, with radius b. The refractive indices of the media within and outside the rhabdomere are n_1 and n_2, respectively. Point P of Fig. 1 is indicated in the cylindrical coordinates of the rhabdomere

where $R = r/b$ is the radial distance from the waveguide axis, r, normalized to its radius value, b; φ is the radial angle; J_l and K_l are (modified) Bessel functions (Fig. 6a, b). The values of U and W are intimately linked to the mode propagation constant, β, given by:

$$\beta = n_e k = \sqrt{n_1^2 k^2 - \left(\frac{U}{b}\right)^2} = \sqrt{n_2^2 k^2 + \left(\frac{W}{b}\right)^2} \qquad (16)$$

where n_e is the effective refractive index of the waveguide for the propagated mode, and U and W are the roots of the characteristic equation:

$$U\frac{J_{l+1}(U)}{J_l(U)} = W\frac{K_{l+1}(W)}{K_l(W)} \qquad (17)$$

Equation 16 immediately yields that U and W together determine the crucially important waveguide number V:

$$V = \sqrt{U^2 + W^2} = kb\sqrt{(n_1^2 - n_2^2)} = \frac{\pi D_r}{\lambda}\sqrt{(n_1^2 - n_2^2)} \qquad (18)$$

where $D_r = 2b$ is the diameter of the rhabdomere. The V-number hence is determined by four parameters, i.e., the wavelength λ, the waveguide diameter D_r, and the refractive indices n_1 and n_2 of the inside and outside media (Snyder 1969).

Table 1 shows that the V-number for a 4-μm rhabdomere and a wavelength range from 300 nm to 600 nm ranges to well over 10 (taking for the refractive indices of the media within and surrounding the rhabdomere values $n_1 = 1.363$ and $n_2 = 1.340$, respectively). The roots of the characteristic equation (Eq. 17) have therefore been calculated for the range $0 < V < 11$ (Fig. 7).

As follows from Eq. 15a, the number of zeros in the azimuthal direction, i.e., for $0 < \varphi < 2\pi$, is given by l. For each value of l, Eq. 17 appears to have several roots, which are indicated by a rank number, m (Gloge 1971; Yariv 1985). The value of m of the different modes existing for a certain value of l increases with V_{co}, the mode's cut-off value of the waveguide number (see Table 2). For clarity's sake, I have renumbered the modes with a single index p according to an increasing value of V_{co}; see Fig. 7 and Table 2.

The factor N_p in Eq. 14 is a normalization constant, which depends on the total power transported by the mode. A useful case to consider is that when mode p transports unit light power: P* = 1 W. The light intensity in a point P(R,φ) (Fig. 5) is given by:

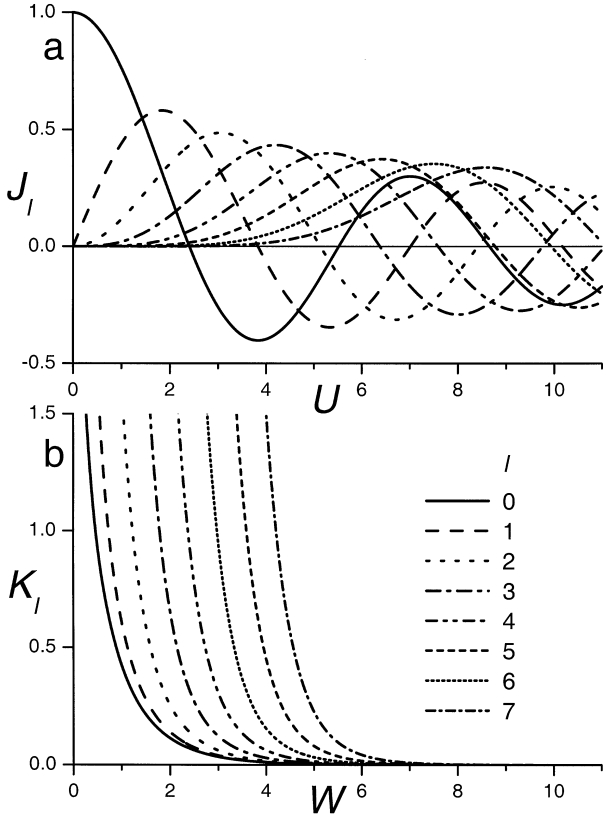

Fig. 6 The Bessel functions J_l (**a**) and K_l (**b**) which together with the characteristic equation (Eq. 17) determine the roots, U and W, as a function of the waveguide number, V

Table 1 Values of the V-number for three values of the rhabdomere diameter, D_r, and four wavelengths, λ, calculated from Eq. 18 with refractive index values $n_1 = 1.363$ and $n_2 = 1.340$

λ (nm)	1 μm	2 μm	4 μm
300	2.61	5.22	10.44
400	1.96	3.92	7.83
500	1.57	3.13	6.27
600	1.31	2.61	5.22

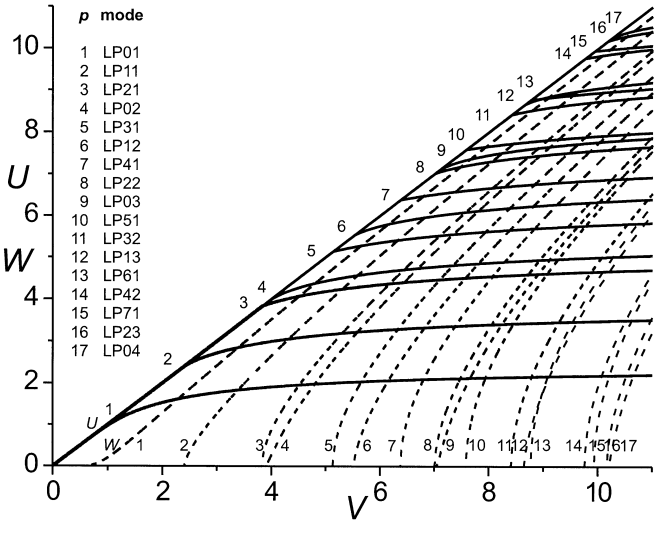

Fig. 7 The roots of the characteristic equation (Eq. 17) determine the spatial shape of the bound modes, indicated by the parameter p. The modes are linearly polarized modes, LPlm, where l is the number of azimuthal zeros and m is the rank number of the modes existing for each value of l. 17 different bound modes exist for $V = 11$. U solid lines; W dashed lines

Table 2 Linearly polarized waveguide modes with mode number p, azimuthal number l, rank number m, and cut-off V-number V_{co}

p	l	m	mode	V_{co}
1	0	1	LP01	0
2	1	1	LP11	2.4050
3	2	1	LP21	3.8318
4	0	2	LP02	3.8473
5	3	1	LP31	5.1357
6	1	2	LP12	5.5201
7	4	1	LP41	6.3802
8	2	2	LP22	7.0156
9	0	3	LP03	7.0247
10	5	1	LP51	7.5883
11	3	2	LP32	8.4173
12	1	3	LP13	8.6538
13	6	1	LP61	8.7715
14	4	2	LP42	9.7611
15	7	1	LP71	9.9362
16	2	3	LP23	10.1735
17	0	4	LP04	10.1799

$$I_p(R,\varphi) = \frac{1}{2}\frac{n_e}{\zeta}\left|e_p(R,\varphi)\right|^2 \tag{19}$$

where ζ is the impedance of free space. The light power propagated in the waveguide core ($R < 1$) is:

$$P_i^* = b^2 \int_0^1 RdR \int_0^{2\pi} I_p(R,\varphi)d\varphi = \frac{\pi b^2}{4}\frac{n_e}{\zeta}\frac{c_p}{N_p} \times \left[J_l^2(U) - J_{l-1}(U)J_{l+1}(U)\right] \tag{20}$$

and that in the outside medium ($R > 1$) is:

$$P_o^* = b^2 \int_1^\infty RdR \int_0^{2\pi} I_p(R,\varphi)d\varphi = -\frac{\pi b^2}{4}\frac{n_e}{\zeta}\frac{c_p}{N_p} \times \left[J_l^2(U) + \frac{U^2}{W^2}J_{l-1}(U)J_{l+1}(U)\right] \tag{21}$$

with $c_p = 2$ for $l = 0$ (i.e., for $p = 1, 4, 9, 17,...$) and $c_p = 1$ for $l = 1, 2, ...$ (i.e., for $p = 2, 3, 5–8, 10–16, ...$); see Fig. 7 and Table 2. The condition $P^* = P_i^* + P_o^* = 1$ W yields the normalization coefficient (Marcuse 1974):

$$N_p = -\frac{\pi b^2}{4}\frac{n_e}{\zeta}c_p\frac{V^2}{W^2}J_{l-1}(U)J_{l+1}(U) \tag{22}$$

The expression for the light intensity (Eq. 19) then becomes:

$$I_p(R,\varphi) = -\frac{2}{\pi b^2}\frac{1}{c_p}\frac{W^2}{V^2}\frac{1}{J_{l-1}(U)J_{l+1}(U)}\left|M_p(R)\right|^2\cos^2(l\varphi) \tag{23}$$

where $U = U_p(V)$ and $W = W_p(V)$ are derived from Eq. 17 (Figure 7). Equation 23 thus fully describes the light distribution in a mode with the light polarized along the x-axis. Incident light is commonly unpolarized, and it is therefore useful to also consider the average intensity at distance R from the waveguide center ($c_p = 2$ for $l = 0$ and $c_p = 1$ for $l = 1, 2, ...$):

$$\bar{I}_p(R) = -\frac{1}{\pi b^2}\frac{W^2}{V^2}\frac{1}{J_{l-1}(U)J_{l+1}(U)}\left|M_p(R)\right|^2 \tag{24}$$

Because visual pigment is concentrated within the rhabdomere, light can be absorbed only from the light wave within the rhabdomere boundary. The fraction of the light power propagated inside the optical waveguide by mode p, P_i^*/P^*, is:

$$\eta_p = \frac{W^2}{V^2}\left(1 - \frac{J_l^2(U)}{J_{l-1}(U)J_{l+1}(U)}\right) \tag{25}$$

Optical waveguide modes in a fly rhabdomere

When the rhabdomere diameter is known, its V-number is fully determined by the light wavelength. The light distribution of all modes p then can be immediately calculated from Eq. 23, together with Eqs. 14 and 15, since $U_p(V)$ and $W_p(V)$ are known for each waveguide mode p (Fig. 7; the azimuthal parameter, l, of mode p is taken from Table 2). As a rhabdomere with diameter $D_r = 4$ μm has at 300 nm a V-number of 10.44 (Table 1), it can thus propagate light of 300 nm in 17 different modes (Fig. 7, Table 2). Figure 8 presents the 3-D intensity profiles of 13 of these 17 modes, arranged in rows with $l = 0$, 1, 2, 3, and 4, and columns with $m = 1$, 2, and 3. For each of the presented modes, the total, integrated light power is 1 W. For comparison, the profile in the right hand lower corner pictures a situation where all the light power is confined within the rhabdomere boundary, with a constant intensity, thus being $4/(\pi D_r^2) = 1/4\pi$ W μm^{-2}.

The circular symmetrical mode patterns in the upper row of Fig. 8 are readily recognized to be due to the value of l, as $\cos(l\varphi) = 1$ for $l = 0$ (Eq. 14). The radial dependence of the mode patterns is determined by the Bessel function $J_0(UR)$ for $0 < R < 1$ (Eq. 15a; Fig. 6a) and by $K_0(WR)$ for $R > 1$ (Eq. 15b; Fig. 6b), where the values of U and W can be read off Fig. 7 at $V = 10.44$ for modes $p = 1$, 4, and 9, respectively. Similarly, the shape of the patterns in the second (third, etc.) row are determined by $J_l(UR)$, $K_l(WR)$, and $\cos(l\varphi)$, with $l = 1$ (2, etc.).

Figure 9 presents η_p (Eq. 25), the light fraction which is propagated by a mode within the rhabdomere boundary, for three cases, i.e., for rhabdomeres with diameter $D_r = 1.0$, 2.0, and 4.0 μm, respectively. An increasing number of bound modes can exist with increasing V-number (Fig. 7), or with increasing rhabdomere diameter and decreasing wavelength (Fig. 9). For most of the modes $\eta_p = 0$ at the cut-off wavelength, but

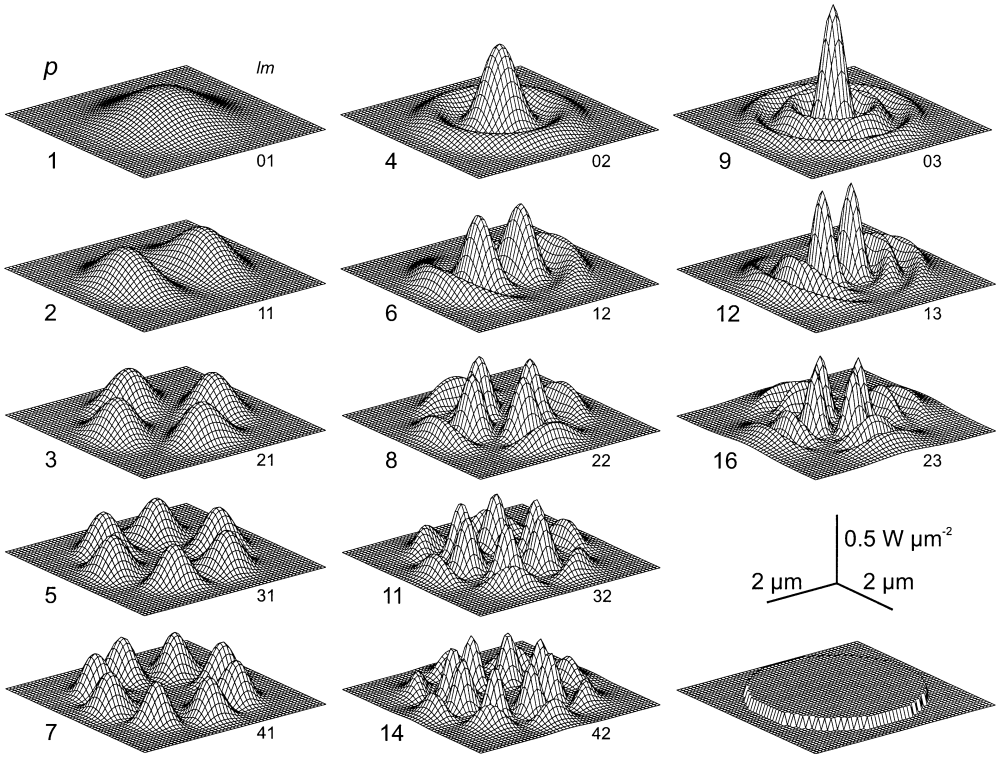

Fig. 8 Spatial intensity profiles for 13 of the 17 modes allowed by a fly rhabdomere with diameter 4 μm at 300 nm. The mode number, p, is indicated at *left* below each profile and the corresponding l- and m-value pair is given at *right*. The total power of each mode is 1 W. The *unnumbered profile* in the right hand lower corner represents the case when the light power is constant and confined within the rhabdom boundary, so that the intensity there is $1/4\pi$ W μm^{-2}

modes 3, 5, 7, 8, 10, 11, and 13–16 have a special behavior, as $\eta_p > 0$ at cut-off (Fig. 9). Above their cut-off wavelength these modes are no longer bound, but become leaky (see Snyder and Love 1983).

The light fraction propagating outside the rhabdomere increases with increasing mode number p (Fig. 9). This is visualized with more detail in Fig. 10, showing the average radial intensity distribution of the modes (Eq. 24) for a rhabdomere with diameter 2 μm, for four different wavelengths. Whereas at 600 nm only two modes are allowed, at 300 nm five modes exist (Fig. 9b). The higher the mode number, the more the light wave extends beyond the waveguide border.

All modes in Figs. 8 and 10 have a total power of 1 W. When a total power of 1 W enters the facet lens and subsequently is channeled into the rhabdomere, the light power in the waveguide is distributed over the various modes, however, and the power carried by each mode crucially depends on the light distribution at the entrance of the waveguide, as will be discussed below.

Excitation of modes in a waveguide by a focusing lens

Light focused by a facet lens and entering a rhabdomere excites a set of waveguide modes. Mode excitation depends on the electromagnetic field at the waveguide entrance and therefore we have to convert the scalar field into the equivalent electric and magnetic field (cf. Barrell and Pask 1979). When the incident light, emitted by a point source at infinity, is polarized along the x-axis (Fig. 5), and E_x is the amplitude of the electric field in the image principal plane of the facet lens, the amplitude of the magnetic field is:

$$H_y = \frac{n'}{\zeta} E_x = \frac{1}{\zeta'} E_x \tag{26}$$

where ζ and ζ' are the impedances of free and image space, respectively. The light intensity, i.e., the time averaged light power density, is:

$$\overline{S}_z = \frac{1}{2} E_x H_y^* = \frac{1}{2\zeta'} |E_x|^2 \tag{27}$$

We have seen above that the light intensity in the image principal plane of the lens is I_a (Eq. 2), with Q_a the amplitude of the diffracted field (Eq. 1). Therefore:

$$E_x = \sqrt{2\zeta'} Q_a \tag{28}$$

Similarly, the field in a point P = P(s,z) (Fig. 5) is:

$$E(s,z) = \sqrt{2\zeta'} Q(s,z) \tag{29}$$

where $Q(s,z)$ is given by Eq. 6.

The diffracted field in the entrance plane of a waveguide excites the waveguide modes described by the modal excitation coefficient, a_p, defined by (Barrell and Pask 1979):

$$a_p(\theta) = \frac{n_e}{2\zeta} \int_0^\infty r dr \int_0^{2\pi} E(s,z) e_p(r,\varphi) d\varphi \tag{30}$$

where

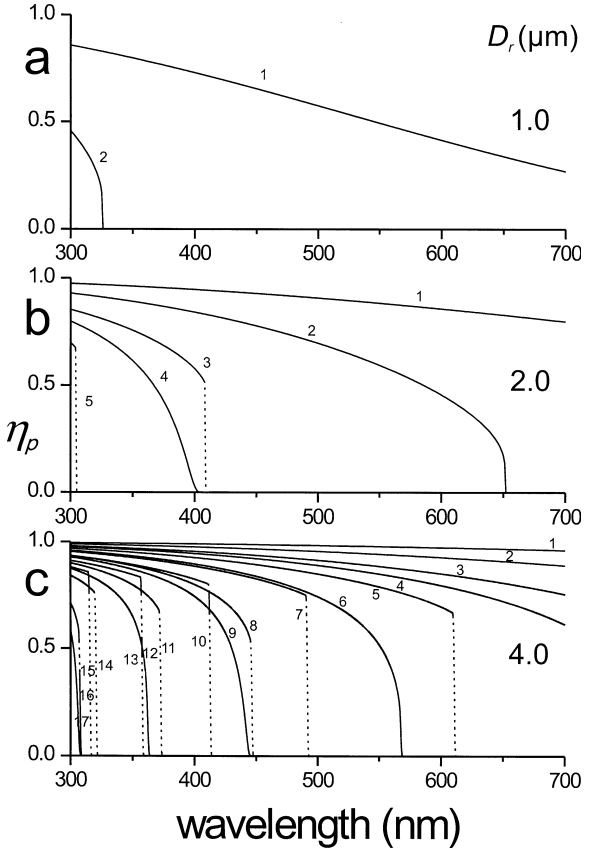

Fig. 9 The fraction of the light power propagated within the rhabdomere boundary, η_p, when the rhabdomere diameter is 1.0 (**a**), 2.0 (**b**), and 4.0 μm (**c**) as a function of wavelength. The allowed modes are indicated by their *p*-value. The number of allowed modes increases with increasing rhabdomere diameter and decreasing wavelength; the light fraction η_p for a certain mode increases with decreasing wavelength. The light fraction η_p of modes 3, 5, 7, 8, 10, 11, and 13–16 is > 0 at the cut-off wavelengths

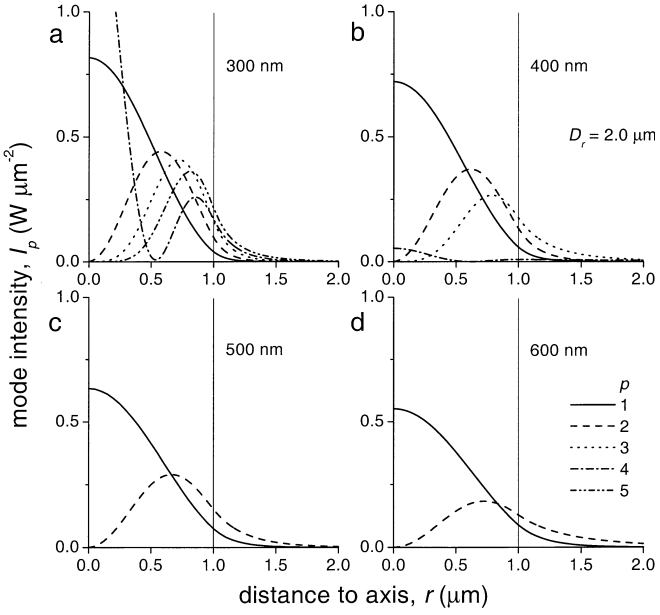

Fig. 10 Radial dependence of the average mode intensity in a rhabdomere with diameter 2.0 μm for four wavelengths: 300 (**a**), 400 (**b**), 500 (**c**), and 600 nm (**d**). The *thin vertical lines* indicate the rhabdomere border. The higher-order modes increasingly extend further to outside the rhabdomere. The total power of each mode is 1 W

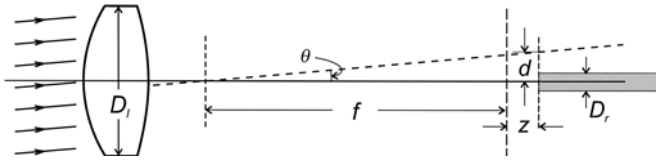

Fig. 11 Diagram of the integrated facet lens – rhabdomere system. A parallel light beam, emitted by a point source at infinity enters the lens with an angle of incidence θ. The diffracted light will excite modes in a rhabdomere, with diameter D_r, whose tip is located at a distance z from the image focal plane. f is the object focal distance, and d is the distance to the axis of the point where the light beam strikes the rhabdomere entrance plane: $d = (f + z)\tan\theta$

$$\theta = \arctan\left(\frac{d}{f+z}\right) \tag{31}$$

with d the distance of the point to the lens axis where the beam axis crosses the plane of the waveguide entrance (Fig. 11).

The modal excitation coefficient can be obtained numerically from Eq. 30. The considerable computer time involved is substantially reduced by a formalism derived by Barrell and Pask (1979). They considered the excitation of waveguide modes by the diffracted field of a classical lens, i.e., with a high Fresnel-number, or, for $\delta = 1$ (Eq. 7e). By using the radius of the waveguide, b, they introduced a number of parameters:

$$K' = k'b,\ S = s/b,\ \text{and}\ Z = z/b, \tag{32}$$

yielding for the electric field in P(S,Z):

$$E(S,Z) = -i\sqrt{\frac{2\zeta'}{\pi}}\frac{1}{bK'q'}e^{i\Phi}\int_0^{K'q'} J_0(S\Omega)e^{-i\frac{Z\Omega^2}{2K'}}\Omega d\Omega \tag{33}$$

with $\Phi = k'z = K'Z$. Then Eq. 30 is equivalent to, with Eqs. 14, 15, 22, and 33:

$$a_p(\theta) = -\frac{2}{K'q'}\frac{W}{V}\sqrt{\frac{2n_e}{c_p n' J_{l-1}(U)J_{l+1}(U)}}e^{i\Phi} \int_0^{K'q'} J_l(D\Omega)G(\Omega)e^{-i\frac{Z\Omega^2}{2K'}}\Omega d\Omega \tag{34}$$

where $D = d/b = (f + z)(\tan\theta)/\mathrm{b}$, and

$$G(\Omega) = \frac{V^2}{(\Omega^2 - U^2)(\Omega^2 + W^2)} [\Omega J_l(U)J_{l+1}(\Omega) - UJ_l(\Omega)J_{l+1}(U)]\ \ (\Omega \neq \mathrm{U}) \tag{35a}$$

or

$$G(\Omega) = \frac{1}{2}\left[J_l^2(U) - J_{l-1}(U)J_{l+1}(U)\right] \quad (\Omega = \mathrm{U}) \qquad (35b)$$

Equation 34 very slightly differs from the final expression (Eq. 16) of Barrell and Pask (1979); as in Eq. 79 of Snyder (1969), Barrell and Pask (1979) do not incorporate a factor 1/2 when using orthonormalization. Furthermore, the exponential under their integral lacks a minus sign, but that is without effect when considering lens diffraction at high Fresnel numbers, because of the symmetry with respect to the focal plane. The special situation of Eq. 35b is explicitly given by van Hateren (1984), but not by Barrell and Pask (1979).

As Eq. 34 has been derived for high Fresnel-number lenses, it may no longer be adequate when the Fresnel number is small, which is the case for fly facet lenses. Fortunately Eq. 34 can be rescued by redefining K' as $K' = k'b/\delta$ and assuming that the effect of the radial dependence of Φ, emerging at small Fresnel numbers (Eq. 7d), remains negligible. Comparing calculations of the excitation of waveguide modes using the generic equation Eq. 30 with results from Eq. 34 where the modified K' is incorporated shows that Eqs. 30 and 34 yield virtually identical results in a wide region around the focal point.

In general, a light wave propagating in an optical waveguide will be a superposition of modes with amplitudes a_p. The total field of the modes is then (Barrell and Pask 1979):

$$\mathbf{E}_{tot} = \sum_p a_p \mathbf{e}_p \qquad (36)$$

The total excited power carried by the modes is, due to orthonormality, equal to the sum of the power of the individual modes (Pask and Barrell 1980a):

$$P_{exc} = \sum_p |a_p|^2 = \sum_p P_{p,exc} \qquad (37)$$

The total flow of light power therefore can be directly obtained by calculating the contribution of the bound modes from their modal excitation coefficients, a_p (Eq. 34; see Eq. 21 of van Hateren 1984). The phase factor $e^{i\Phi}$ in Eq. 34 vanishes when calculating the absorbed light power. Van Hateren (1984) has treated mode excitation with the waveguide entrance in the focal plane. The exponential function under the integral in Eq. 34 then vanishes, because $Z = 0$.

Equation 34 reveals that the angular dependence of the mode excitation depends on several parameters, the relative importance of which can be assessed numerically. A few selected cases are treated below.

Excitation of waveguide modes in a fly rhabdomere illuminated via a facet lens

Figure 12 shows how mode excitation depends on the position of the rhabdomere tip for a 40-μm facet lens combined with a 2μm rhabdomere. The four columns concern light of the four wavelengths, 300, 400, 500, and 600 nm, and the five rows concern five positions of the rhabdomere, where the middle row gives the situation that the rhabdomere tip coincides with the image focal plane and the other rows show the excited mode power when the tip is 5 μm and 10 μm distally or proximally of the focal plane. The thin vertical lines indicate the specific angle of incidence where the axis of the incident light beam hits the rhabdomere border (see Fig. 11):

$$\theta_0 = \arctan\left(\frac{b}{f+z}\right) \qquad (38)$$

Mode excitation clearly depends on the angle of incidence (Fig. 12). Axial illumination with 500 nm and 600 nm light excites only the first mode ($p = 1$), but with increasing off-axis illumination the second mode ($p = 2$) progressively comes in. The total excited light power, being the sum of the power channeled into the individual modes, has an approximately Gaussian-shaped dependence on the angle of incidence. At 400 nm and 300 nm, four and five modes participate, respectively. The angular dependence of the total mode power excited distinctly deviates from a Gaussian at the shorter wavelengths, due to the relatively large contributions of the higher order modes at off-axis illuminations. The amplitude of the excited mode power gradually diminishes when the distance of the rhabdomere tip to the focal plane increases, which is accompanied by an angular broadening of the mode power function (Fig. 12).

According to general dogma, light capture by the visual pigments in the rhabdomere should be optimized, and hence Fig. 13 further investigates how careful flies must be in positioning the rhabdomere tip in the focal plane. Three facet lenses with diameter 20, 40 and 80 μm are combined with rhabdomeres having a diameter of 1, 2, and 4 μm, respectively, or, in all three cases $D_l/D_r = 20$. Figure 13 gives the total mode power as a function of the distance of the rhabdomere tip to the focal plane, for the case when the angle of the incident light is $\theta = 0°$ (axial illumination), for the four wavelengths: 300, 400, 500 and 600 nm.

The excited mode power is maximal when the rhabdomere tip is precisely in the focal plane, for all lens-rhabdomere combinations and for all wavelengths. This might not have been directly expected, as the diffraction patterns exhibit a focal shift; namely, the intensity maximum is located distal to the focal point, especially for the shorter wavelengths and the smaller lenses (Fig. 3). In fact, the curves of Fig. 13 show a slight asymmetry with respect to the focal point, opposite to that of the diffraction patterns of Fig. 3, quite contrary to the expectation that the excited power might be higher with a rhabdomere tip shifted distally from the focal plane. The excited mode power appears to depend somewhat on the light wavelength, but the wavelength dependence is minor for the large rhabdomere

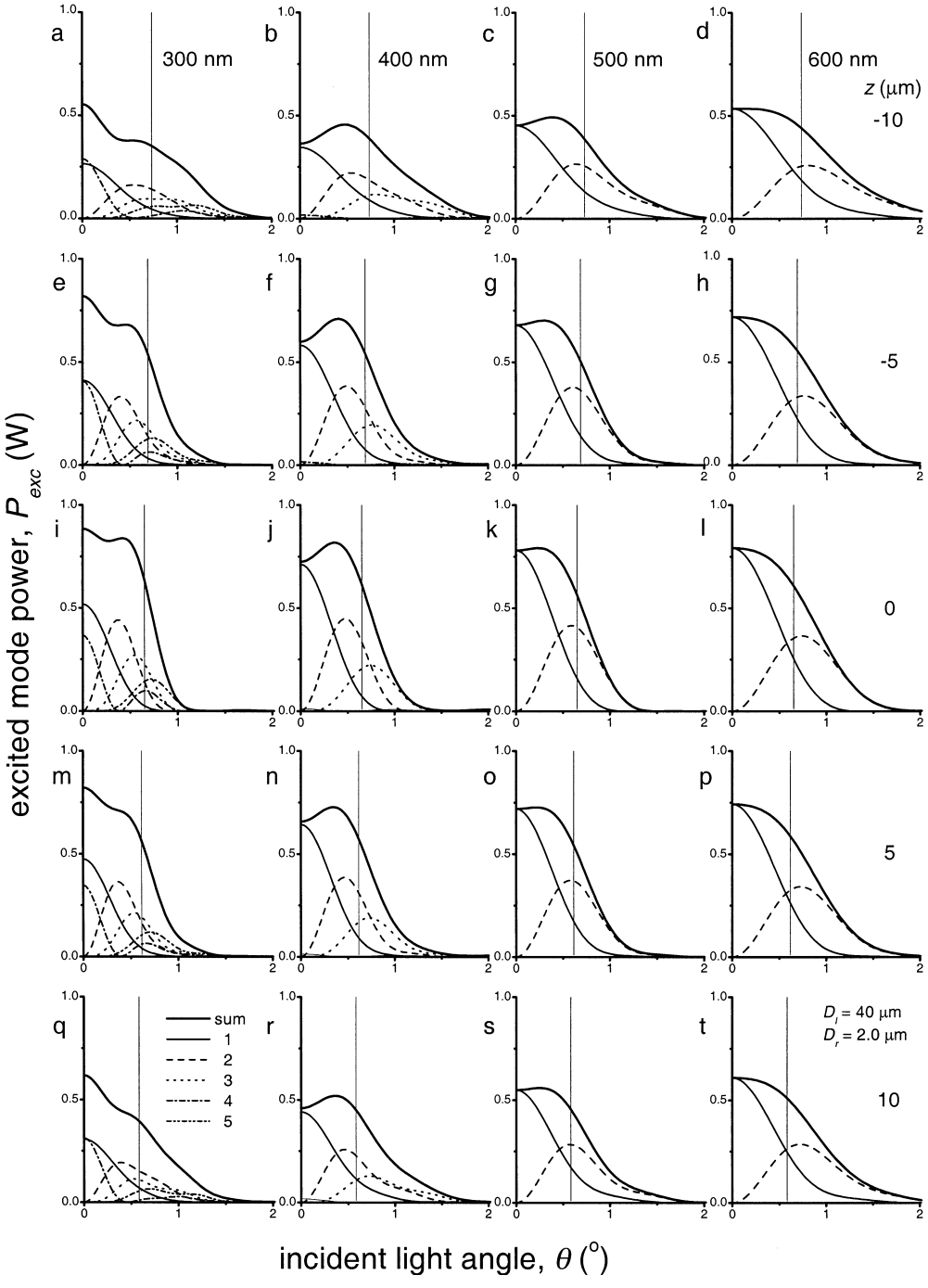

Fig. 12 The mode power excited as a function of light incidence for a facet lens-rhabdomere combination where the diameters of the lens and rhabdomere are 40 μm and 2.0 μm, respectively, and where the rhabdomere tip is positioned in a plane at a distance of $z = -10$ (**a**–**d**), –5 (**e**–**h**), 0 (**i**–**l**), 5 (**m**–**p**), and 10 μm (**q**–**t**) from the image focal plane. The four columns concern light with wavelengths 300, 400, 500, and 600 nm, respectively. The mode power excited in the allowed modes is indicated together with their sum, the total excited power (*bold lines*). The *thin vertical lines* indicate the border angle of incidence, i.e., when the incident light beam strikes the rhabdomere border: $\theta_0 = \arctan(1/(88 + z))$

(Fig. 13c). This is again quite in contrast with the diffraction patterns where the intensity is inversely proportional to the square of the wavelength (Figs. 2, 3, 4). The wavelength dependence of lens diffraction is clearly well compensated by the wavelength dependence of mode propagation in the waveguide (see also van Hateren 1989).

With the rhabdomere tip in the focal plane, the maximal value of the total excited mode power gradually increases with the size of the rhabdomere, but it never reaches 1 W, the total incident light power. Some light always escapes capture by the rhabdomere. This loss fraction increases when the rhabdomere tip leaves the focal plane. In the case of the small rhabdomere (Fig. 13a) light capture falls rapidly when defocus is more than a few μm, but the sensitivity of the large rhabdomere (Figure 13c) remains fairly constant when the rhabdomere tip is shifted over a longitudinal distance of 10 μm. These effects are fully due to the size of the rhabdomere, as the diffraction patterns are very similar in the three cases, because of their identical F-number (see Fig. 3).

The reason why not all incident light power can be launched into the rhabdomere is visualized in Fig. 14.

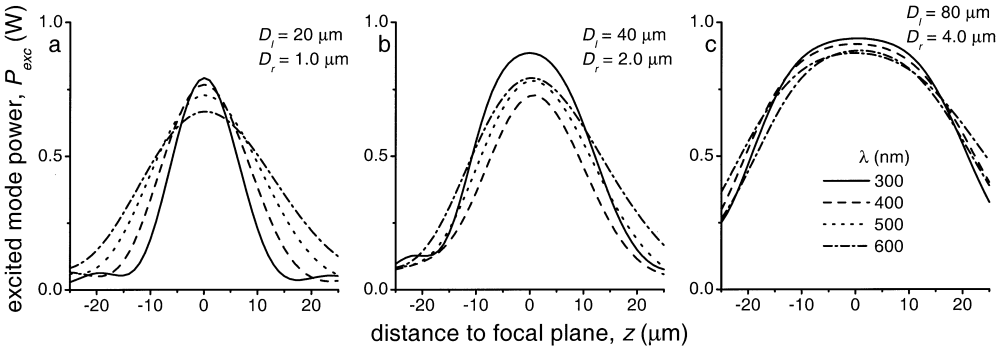

Fig. 13 The total excited mode power for three lens-rhabdomere sets, with diameters 20 (**a**), 40 (**b**), and 80 μm (**c**) paired with rhabdomeres with diameter 1.0 (**a**), 2.0 (**b**), and 4.0 μm (**c**), respectively, for four wavelengths: 300, 400, 500, and 600 nm. The rhabdomere is centered at the lens axis and the incident illumination beam is parallel to the axis. The tip of the rhabdomere is positioned at a distance z from the image focal plane. The excited power is maximal when the rhabdomere tip coincides with the focal plane in all cases. It stays virtually constant when the rhabdomere changes position over a few micrometers, especially for the large rhabdomere

Figure 14a shows the amplitude distribution in the focal plane of the 40-μm facet lens due to an axially incident light wave with wavelength 500 nm. The amplitude distribution closely approximates that of the classical Airy expression (cf. Eqs. 9 and 10): for distances $|s| < 3$ μm. The amplitude distribution of mode 1, excited in the 2.0μm rhabdomere (the borders of which are indicated by the thin vertical lines), largely but incompletely matches the diffraction function. When the incident angle is equal to the border angle θ_0 (Eq. 38) both mode 1 and mode 2 are excited (Fig. 14b), and their sum, being the best possible match, is clearly distinctly worse. Note that the amplitude distributions are rotational symmetric for the diffraction pattern and mode 1, but not for mode 2. For a 3-D presentation, giving a more complete picture of the convolution of diffraction and mode patterns, see van Hateren (1989) and Warrant and McIntyre (1993).

Figure 15 investigates the dependence of the total excited mode power on the angle of light incidence for four wavelengths. The total launched power is given for the same three facet lens-rhabdomere combinations as those of Fig. 13, with the rhabdomere tip in the focal plane ($z = 0$). The border angle (Eq. 38), indicated by the thin vertical line in Fig. 15a–c, is identical for the three cases, because $b/f = D_r/(2FD_l) = 1/88$, or $\theta_0 = 0.65°$. The four curves in Fig. 15b represent the same functions as the four bold curves in Fig. 12i–l. It appears that the angular dependence of the total excited light power noticeably varies with wavelength for the 1.0-μm rhabdomere; the wavelength dependence is minor for the large rhabdomere.

Fig. 14 Amplitude distributions of the diffracted light wave in the focal plane of a 40μm lens and the excited modes in a 2.0μm rhabdomere. **a** Incident light wave parallel to the lens axis. Only mode 1 is excited, matching the diffraction distribution rather well. **b** Angle of incidence of the light wave equal to the border angle $\theta_0 = \tan(1/88) = 0.65°$. Both mode 1 and mode 2 are excited, but the amplitudes of the modes are low. The sum of the mode amplitudes resembles the amplitude of the diffraction distribution

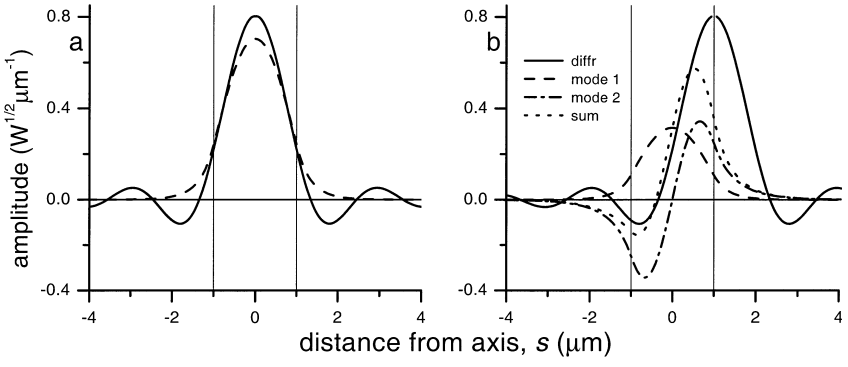

Light absorption in an optical waveguide

The aim of light propagation in a fly rhabdomere is the absorption of light by the visual pigment molecules embedded in the microvillar membranes. This is the primary step in vision. The visual pigment is confined to the interior medium of the rhabdomere and thus can only absorb light propagated within the rhabdomere boundary.

Consider light of wavelength λ propagated in the rhabdomere. The power of mode p in the rhabdomere is then given by $P_p(\lambda, z)$, where z is the longitudinal coordinate of the rhabdomere, and $z = 0$ when the rhabdomere tip is in the focal plane. The light absorption is then given by (Snyder 1979):

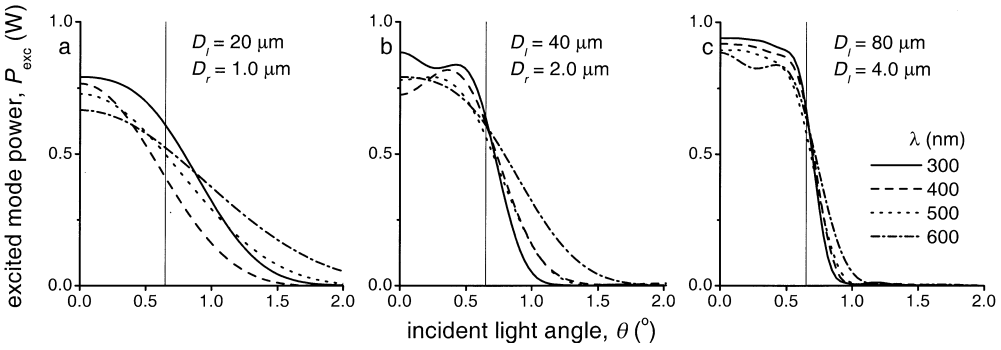

Fig. 15 The total excited power as a function of the incident angle for the same lens-rhabdomere pairs as in Fig. 12, with the rhabdomere in the focal plane ($z = 0$). The *thin vertical lines* indicate the border angle, where $\theta_0 = 0.65°$. The angular dependencies are rather similar, especially for the large rhabdomere

$$dP_p(\lambda, z) = -P_p(\lambda, z)\eta_p(\lambda)\kappa(\lambda)dz \tag{39}$$

where $\kappa(\lambda)$ is the specific absorption coefficient of the rhabdomere medium containing the visual pigment and $\eta_p(\lambda)$ the fraction of the mode power within the rhabdomere (Eq. 25). When the excited light power of mode p is $P_{p,exc}(\lambda)$, the amount absorbed from it in a rhabdomere with length L is (Snyder and Pask 1973):

$$P_{p,abs}(\lambda) = P_{p,exc}(\lambda)\left\{1 - e^{-\eta_p(\lambda)\kappa(\lambda)L}\right\} \tag{40}$$

If the radius of the waveguide is not constant, i.e., $b = b(z)$ and $\eta_p(\lambda) = \eta_p(\lambda, z)$; then $\eta_p(\lambda)$ in Eq. 40 has to be replaced by the averaged value (Snyder and Pask 1973):

$$\bar{\eta}_p = \frac{1}{L}\int_0^L \eta_p(\lambda, z)dz \tag{41}$$

The total absorbed light power is calculated by taking the sum over the propagated modes (Pask and Barrell 1980a):

$$P_{abs}(\lambda) = \sum_p P_{p,abs}(\lambda) \tag{42}$$

Photoreceptor angular sensitivity when absorption is low

When each absorbed photon contributes equally to the photoreceptor response, the angular sensitivity is obtained by normalizing the absorbed power. A full analysis of the angular sensitivity of fly rhabdomeres has to be elaborated elsewhere, because many complicating factors must be taken into account, e.g., the spectral dependence of the absorption coefficient of the visual pigment, including the presence of a sensitizing pigment and/or filtering pigments, the possible effects of photoproducts, the rhabdomere length differing between species, the tapering of the R1–6 rhabdomeres (Boschek 1971), the tiered positioning of the R7 and R8 rhabdomeres (Hardie 1985), and the effect of a pupil mechanism in the light-adapted state (Fig. 1a, b; Smakman et al. 1984). Considerable insight can nevertheless easily be gained from the special case that the diameter of the rhabdomere is constant and the absorption coefficient is sufficiently small to neglect the self-screening effects due to the exponential function in Eq. 40. The dependence of the absorption on the angle of incidence, θ, is then given by (Pask and Barrell 1980a):

$$P_{p,abs}(\theta, \lambda) = P_{p,exc}(\theta, \lambda)\eta_p(\lambda)\kappa(\lambda)L \tag{43}$$

where $P_{p,exc}(\theta, \lambda)$ is again the excited mode power as a function of angle and wavelength. Eq. 42 then yields:

$$P_{abs}(\theta, \lambda) = \kappa(\lambda)L\sum_p P_{p,exc}(\theta, \lambda)\eta_p(\lambda) = \kappa(\lambda)LP_{eff}(\theta, \lambda) \tag{44}$$

with

$$P_{eff}(\theta, \lambda) = \sum P_{p,eff}(\theta, \lambda) = \sum P_{p,exc}(\theta, \lambda)\eta_p(\lambda) \tag{45}$$

where $P_{p,eff}$ is the effective light power of mode p, and P_{eff} is the total effective light power.

Figure 16 presents the effective mode powers for the case of the 40μm facet lens with the tip of the 2μm rhabdomere in its focal plane. Their sum, the total effective light power, given by the bold curve, is compared with the total excited power, given by the dotted curve (Fig. 12i–l). The reduced absorption of the higher-order modes has a smoothing effect on the angular dependence. It may be anticipated that this effect is enhanced with increased absorption by the visual pigment, especially in a tapering rhabdomere (Pask and Barrell 1980b).

This approach is carried one step further in Fig. 17a–c, where $P_{eff}(\theta, \lambda)$ is calculated for the three lens-rhabdomere combinations of Fig. 15. Light absorption in the small rhabdomere clearly suffers from the large fraction of light being propagated outside the rhabdomere boundary, especially at the longer wavelengths. The angular sensitivity is obtained by normalization of the absorbed light power, or equally, by normalization of $P_{eff}(\theta, \lambda)$, because the absorption coefficient, κ, and length L are independent of the angle of incidence (see Eqs. 41, 43, and 44). Figure 17d–f shows that the angular sensitivity thus calculated varies with wavelength.

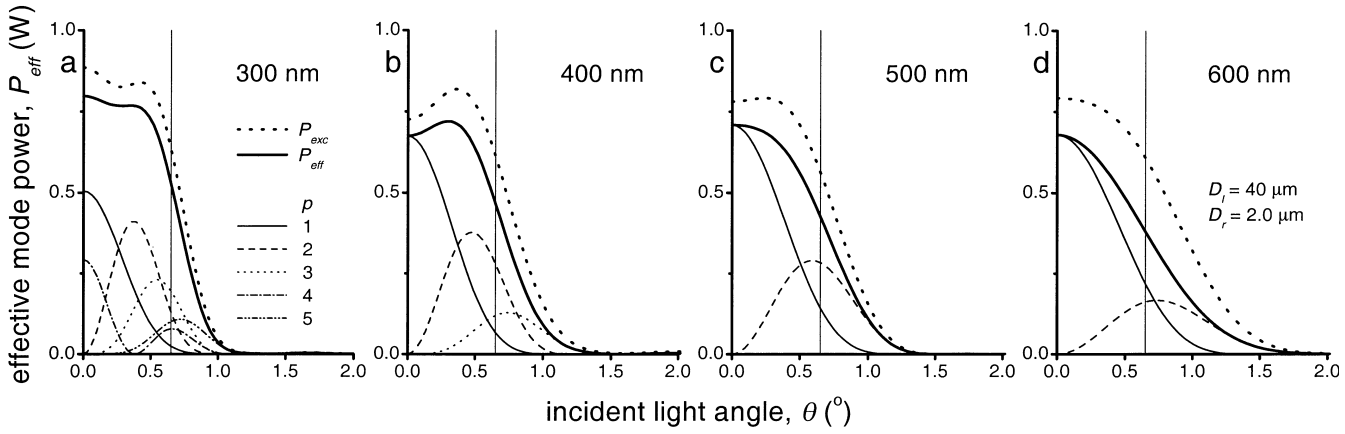

Fig. 16 The effective mode power at wavelengths 300 (**a**), 400 (**b**), 500 (**c**), and 600 nm (**d**), as a function of the incident light angle, for the 40μm facet lens with a 2.0μm rhabdomere in its focal plane. The thin lines represent the effective mode power, $P_{p,eff}$, for each of the modes p (Eq. 45); the *bold continuous lines* give their sum, the total effective power, P_{eff}; and the *upper dotted lines* are the total excited power, P_{exc} (see Fig. 12, panels i–l). The progressive decrease in the light fraction η_p of the higher modes causes the narrowing of the curves for the effective power compared to those of the excited power

The variations may be considered to be rather small, however.

Discussion

The angular sensitivity of photoreceptors is a crucial element determining the performance of a visual system. I have analyzed the angular sensitivity of fly photoreceptors in five steps. Firstly, the diffraction pattern of the facet lenses has been quantitatively presented. Previous experiments have demonstrated that the optics of the facet lenses cannot be properly described by classical diffraction theory, because of their small size (Stavenga and Van Hateren 1991), and therefore the analysis of the angular sensitivity of fly facet lenses by Barrell and Pask (1979) needed a critical re-assessment. The calculations were performed for a number of facet lens diameters typical for the blowflies *Calliphora* and *Chrysomia*, where the diameter ranges from ca 20 μm to 80 μm (Stavenga et al. 1990; van Hateren 1984). Only one value of the F-number, $F = 2.2$, has been considered. The F-number of the facet lenses of the fruitfly, *Drosophila*, is distinctly less: $F = 1.25$ (Franceschini and Kirschfeld 1971). Calculations with the formalism derived in this paper show that a low F-number results in less efficient mode excitation and strongly broadened angular sensitivity curves. The rationale for having a low F-number in *Drosophila* is discussed in a companion paper (Stavenga 2003).

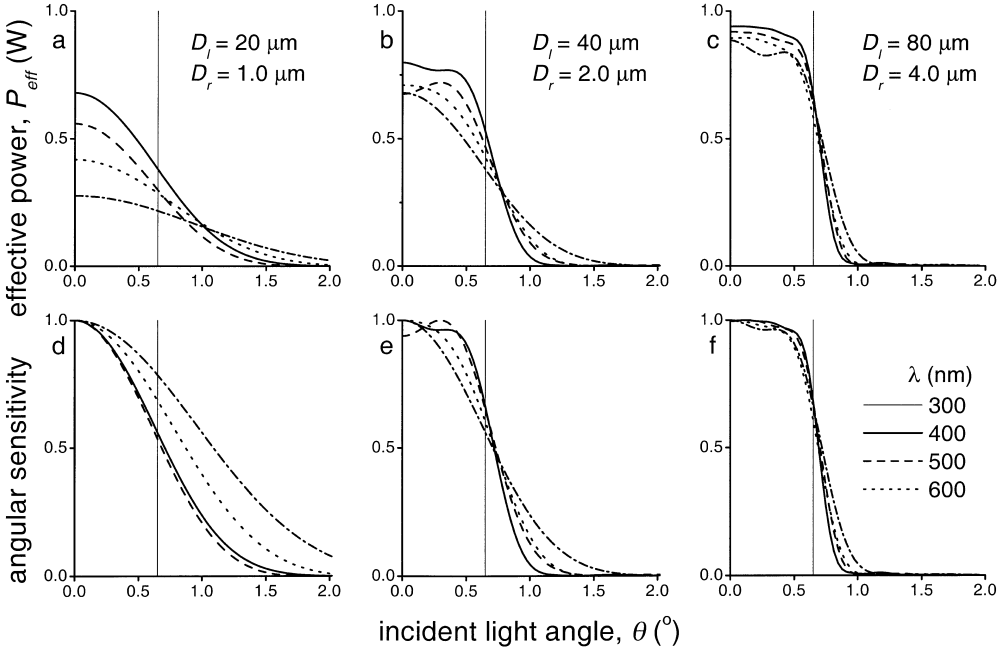

Fig. 17 The effective mode power of the various allowed modes for the three lens-rhabdomere pairs of Figs. 13 and 15 (**a**–**c**) and their normalized values (**d**–**e**). The latter curves represent the angular sensitivities under the assumption that the total light absorption is low. The halfwidths of the curves are similar, especially for the large rhabdomere

In the second part of the analysis, I have shown how light is propagated in rhabdomeres in specific patterns - waveguide modes- using the linearly polarized (LP–) modes approach of Gloge (1971). This approach has its limitations (Snyder and Love 1983), but it is adequate for an analysis of the angular sensitivity (Barrell and Pask 1979; van Hateren 1989). Mode propagation critically depends on the waveguide number, V, which attains values above 10 only for the excessively large rhabdomeres of the male blowfly *Chrysomia* (Table 1). For the more common 1- to 2μm rhabdomeres of other blowflies, and also houseflies and fruitflies, maximal values of about 5 are reached (Table 1). Then at most five modes are allowed to propagate in the ultraviolet, and even fewer for longer wavelengths, depending on V_{co}, the cut-off value of V. [Note that a few values of V_{co} given in Table 2 slightly deviate from those given in the comprehensive treatise of Yariv (1985).]

In the third step I have derived an expression for the amplitude of the modes excited in the rhabdomere by the lens diffraction pattern as a function of the light wave's angle of incidence, extending the formalism of Barrell and Pask (1979) by incorporating the appropriate description of a small diffracting facet lens. The derivation of the modal excitation coefficient a_p (Eq. 34) assumes that the contribution of the distance s in the phase factor Φ (Eq. 7d) is negligible. The error introduced by this approximation appears to be very minor in the region of interest, i.e., near the focal point. Presumably fly rhabdomeres are rather precisely positioned in focus (Franceschini 1975; van Hateren 1989; Stavenga et al. 1996), but fly lenses suffer from slight chromatic aberration (McIntyre and Kirschfeld 1982), causing a wavelength dependence of the focal length of a few μm and hence a wavelength-dependent F-number. Figure 13 shows that the excited power is maximal when the rhabdomere tip coincides with the focal plane, but it appears to be rather robust to changes in the rhabdomere position (see also van Hateren 1985). The consequences of chromatic aberration for the angular sensitivities can hence be neglected (McIntyre and Kirschfeld 1982; Pask and Barrell 1980a). The present analysis indicates that the approach of van Hateren (1984), who analyzed the excitation of waveguide modes in fly rhabdomeres with the entrance positioned in the focal plane, is in principle perfectly adequate.

In the fourth part, I have taken account of light absorption by visual pigment within the rhabdomere. The light power absorbed from a mode equals the excited power times the fraction of light propagated within the rhabdomere, η_p (Snyder and Pask 1973; Pask and Barrell 1980a). Consequently, sensitivity for long-wavelength light is relatively suppressed, especially in slender rhabdomeres (Fig. 17a).

Finally, I have calculated the angular sensitivity by normalizing the angular dependence of the light absorption. The angular sensitivities of Fig. 17d–f are rather similar, although the rhabdomere diameter changes fourfold, which is due to the simultaneous change in facet lens diameter. I have presented those cases where the ratio of lens diameter, D_l, and rhabdomere diameter, D_r, is constant ($D_l/D_r = 20$), to facilitate comparison of the angular sensitivity curves. The angular sensitivities for other combinations can easily be obtained by appropriate scaling, because the diffraction patterns only slightly depend on the facet lens diameter when the F-number is kept constant (Fig. 3). Because of the almost identical diffraction patterns, I conclude that the rhabdomere diameter must be the principal determinant of the slight differences in the resulting angular sensitivities.

The value of the last two steps is somewhat limited, because the calculations have been done for the case of low light absorption, where the Lambert–Beer exponential absorption law can be approximated with the first-order term. This approximation is invalid for a long rhabdomere where the absorption coefficient of the visual pigment is not small. Although the present analysis adequately highlights the major factors shaping the angular sensitivity of fly photoreceptors, a more detailed study, incorporating realistic parameters for rhabdomere geometry and absorption coefficients remains to be executed. For instance, the fraction of light propagated within the rhabdomere, η_p, depends strongly on the rhabdomere diameter, and hence light absorption from the different modes changes along the length in a tapering rhabdomere (Eqs. 41 and 45), which can greatly modify the angular sensitivity (Pask and Barrell 1980b).

The contribution of different waveguide modes to the angular sensitivity has been clearly demonstrated by Smakman et al. (1984). Electrophysiological measurements of the angular sensitivity of blowfly photoreceptors, performed for a number of light wavelengths, could be unequivocally interpreted using Eqs. 34 and 37 (for $z = 0$; see van Hateren 1984), from which values for the radius of the photoreceptor's rhabdomere were obtained. Furthermore, the narrowing of the angular sensitivity curve due to the pupil mechanism, which selectively absorbs higher-order modes, could be readily interpreted. However, the underlying theory (van Hateren 1984) has only considered waveguide mode excitation, which is determined by the distal rhabdomere radius, and has not incorporated the absorbing rhabdomere, whilst the electrophysiologically measured angular sensitivity is determined by the complete, tapering rhabdomere. This criticism does not apply to the angular sensitivities of blowfly photoreceptors measured with optical methods by van Hateren (1984), where the distal ends of the rhabdomeres determine the photographed radiation patterns. However, the derived angular sensitivities then are not fully equivalent to the angular sensitivities of the functional photoreceptors. As outlined above, a complete description must incorporate the rhabdomere tapering and the selective mode absorption. All the same, the experimental data demonstrate that waveguide modes play a crucial role, and that the shape of the angular sensitivity often deviates from a Gaussian function.

Assuming that angular sensitivity functions are Gaussian-shaped, Snyder (1979) introduced an expression for the halfwidth of the angular sensitivity:

$$\Delta\rho = \sqrt{\Delta\rho_l^2 + \Delta\rho_r^2} \quad (46)$$

where $\Delta\rho_l = \lambda/D_l$ accounts for the facet lens diffraction and $\Delta\rho_r = D_r/f$ accounts for the angular acceptance of the rhabdomere. Snyder's formula seems to suggest that the only wavelength-dependent factor is the diffraction by the facet lens and that the contribution by the rhabdomere is wavelength independent. Of course, the waveguide optics of the rhabdomere crucially depends on the light wavelength, but furthermore, the imaging by the two optical components, facet lens and rhabdomere, cannot be separated as they form an integrated-optical system where wave properties dominate. van Hateren (1984) critically assessed Eq. 46 and showed that it distinctly overestimates the actual angular sensitivity. In their profound and broad-ranging treatise of eye design, Warrant and McIntyre (1993) discuss the different optical factors contributing to the angular sensitivity of photoreceptors in arthropod eyes. They clearly illustrate the incorrect treatment of the angular sensitivity by Snyder (1979) and repeatedly reach the conclusion that Eq. 46 inadequately describes the actual angular sensitivity in many photoreceptor systems. The formula nevertheless has been repeatedly used and even favorably advocated recently (Land and Nilsson 2002). It thus appears to be necessary to emphasize here again that Eq. 46, derived with intuitive arguments on a physically incorrect basis, fully neglects the essential wave properties of light that crucially determine the excitation of waveguide modes, that it does not incorporate the differences in absorption from the various waveguide modes, that it does not account for possible tapering of the waveguide, and that it neglects possible selective mode suppression by a pupil mechanism (Warrant and McIntyre 1993).

Equation 46 suggests that the angular sensitivity broadens monotonically with increasing wavelength. This may seem to be the case when the rhabdomere diameter is very small (Fig. 17d), but this is only prominent at long wavelengths, where mode power captured by the rhabdomere (Fig. 17a) as well as absorption by visual pigments is small. In medium and large rhabdomere diameters, the angular sensitivity becomes more squarish for the shorter wavelengths, but the halfwidth then is virtually wavelength independent (Fig. 17e, f). A Gaussian shaped angular sensitivity curve is regained by tapering, but this is then the result from the decreasing absorption from higher waveguide modes (Pask and Barrell 1980b; van Hateren et al. 1989). It thus appears that the angular sensitivity of blowfly and housefly photoreceptors is fully determined by the rhabdomere geometry and that a more adequate expression may be wavelength independent, as has in fact been suggested repeatedly by electrophysiological measurements.

Angular sensitivities have been measured for different wavelengths not only in blowfly but also hoverfly (dark-adapted) photoreceptors, yielding an approximately constant angular sensitivity, varying maximally 10–20% (Horridge et al. 1976; Smakman et al. 1984). The importance of the remaining minor spectral dependencies must be assessed by considering the relative contribution of the various wavelengths to the visual signal. In other words, if we want to understand the optical factors that determine the design of an eye it is essential to explicitly value the spectral weight of the angular sensitivity of a certain wavelength, rather than to consider its normalized spatial function at different wavelengths separately. Vision is performed by photoreceptors containing visual pigments with a spectrally limited bandwidth. A proper treatment of spatial acuity and eye design should therefore define an effective angular sensitivity, which is obtained by normalization after the absorbed light power (Eq. 42) is integrated over the visually relevant wavelength range.

For dark-adapted blowfly photoreceptors, the case of the present paper, such an analysis yields an angular sensitivity well approximated by $\Delta\rho = D_r/f$ over a wide range of lens and rhabdomere diameters (Fig. 17). A generally valid formula, which also covers the partly light-adapted state, may be not within immediate reach however, as the $\Delta\rho$-value decreases when light adaptation activates the pupil mechanism (see Smakman et al. 1984). This should be kept in mind when discussing eye designs, as the partly light-adapted case will be the most commonly occurring situation in a fly's active life. Similar arguments probably hold for most other insect photoreceptors. I tentatively conclude that many optical factors work together to produce an effectively wavelength-independent angular sensitivity function of fly (and other insect) photoreceptors, thereby possibly minimizing interference between the coding of space and color.

Acknowledgements This paper has greatly benefited from discussions and generous comments by Drs. Hans van Hateren, Bernhard Hoenders, Simon Laughlin, and Eric Warrant.

References

Barrell KF, Pask C (1979) Optical fibre excitation by lenses. Optica Acta 26:91–108

Beersma DGM, Hoenders BJ, Huiser AMJ, Toorn P van (1982) Refractive index of the fly rhabdomere. J Opt Soc Am 72:583–588

Born M, Wolf E (1975) Principles of optics, 5th edn. Pergamon Press, Oxford

Boschek B (1971) On the fine structure of the peripheral retina and lamina ganglionaris of the fly, *Musca domestica*. Z Zellforsch 118:369–409

Burton BG, Tatler BW, Laughlin SB (2001) Variations in photoreceptor response dynamics across the fly retina. J Neurophysiol 86:950–960

Franceschini N (1975) Sampling of the visual environment by the compound eye of the fly: fundamentals and applications. In:

Snyder AW, Menzel R (eds) Photoreceptor optics. Springer, Berlin Heidelberg New York, pp 98–125
Franceschini N, Kirschfeld K (1971) Les phénomènes de pseudopupille dans l'oeil composé de *Drosophila*. Kybernetik 9:159–182
Gloge D (1971) Weakly guiding fibres. Appl Opt 10:2252–2258
Götz KG (1964) Optomotorische Untersuchung des visuellen Systems einiger Augenmutanten der Fruchtfliege *Drosophila*. Kybernetik 2:77–92
Hardie RC (1985) Functional organization of the fly retina. In: Ottoson D (ed) Progress in sensory physiology 5. Springer, Berlin Heidelberg New York, pp 1–79
Hateren JH van (1984) Waveguide theory applied to optically measured angular sensitivities of fly photoreceptors. J Comp Physiol A 154:761–771
Hateren JH van (1985) The Stiles-Crawford effect in the eye of the blowfly, *Calliphora erythrocephala*. Vision Res 25:1305–1315
Hateren JH van (1989) Photoreceptor optics, theory and practice. In: Stavenga DG, Hardie RC (eds) Facets of vision. Springer, Berlin Heidelberg New York, pp 74–89
Hateren JH van, Hardie RC, Laughlin SB, Stavenga DG (1989) The bright zone, a specialized dorsal eye region in the male blowfly *Chrysomia megacephala*. J Comp Physiol A 164:297–308
Horridge GA, Mimura K, Hardie RC (1976) Fly photoreceptors. III. Angular sensitivity as a function of wavelength and the limits of resolution. Proc R Soc Lond Ser B 194:151–177
Kuiper JW (1965) On the image formation in a single ommatidium of the compound eye of Diptera. In: Bernhard CG (ed) The functional organization of the compound eye. Pergamon Press, Oxford, pp 35–50
Land MF, Nilsson D-E (2002) Animal eyes. Oxford University Press, Oxford
Li Y, Wolf E (1984) Three-dimensional intensity distribution near the focus in systems of different Fresnel numbers. J Opt Soc Am A 1:801–808
Marcuse D (1974) Theory of dielectric optical waveguides. Academic Press, New York
McIntyre PD, Kirschfeld K (1982) Chromatic aberration of a dipteran corneal lens. J Comp Physiol A 146:493–500
Pask C, Barrell KF (1980a) Photoreceptor optics. I. Introduction to formalism and excitation in a lens-photoreceptor system. Biol Cybern 36:1–8
Pask C, Barrell KF (1980b) Photoreceptor optics. II. Application to angular sensitivity and other properties of a lens-photoreceptor system. Biol Cybern 36:9–18
Seitz G (1968) Der Strahlengang im Appositionsauge von *Calliphora erythrocephala* (Meig.). Z Vergl Physiol 59:205–231
Smakman JG, Hateren JH van, Stavenga DG (1984) Angular sensitivity of blowfly photoreceptors: intracellular measurements and wave-optical predictions. J Comp Physiol A 155:239–247
Snyder AW (1969) Asymptotic expressions for eigenfunctions and eigenvalues of a dielectric or optical waveguide. IEEE Trans Microw Theor Tech 17:1130–1138
Snyder AW (1979) Physics of vision in compound eyes. In: Autrum H (ed) Handbook of Sensory Physiology VII/6A. Springer, Berlin Heidelberg New York, pp 225–313
Snyder AW, Love JD (1983) Optical waveguide theory. Chapman and Hall, London
Snyder AW, Pask C (1973) Spectral sensitivity of dipteran retinula cells. J Comp Physiol 84:59–76
Stavenga DG (1974) Refractive index of fly rhabdomeres. J Comp Physiol 91:417–426
Stavenga DG (1975) Optical qualities of the fly eye – an approach from the side of geometrical, physical and waveguide optics. In: Snyder AW, Menzel R (eds) Photoreceptor optics. Springer, Berlin Heidelberg New York, pp 126–144
Stavenga DG (2003) Angular and spectral sensitivity of fly photoreceptors. II. Dependence on facet lens F-number and rhabdomere type in *Drosophila*. J Comp Physiol A (in press)
Stavenga DG, Barneveld HH van (1975) On dispersion in visual photoreceptors. Vision Res 15:1091–1095
Stavenga DG, Hateren JH van (1991) Focusing by a high power, low Fresnel number lens: the fly facet lens. J Opt Soc Am A 8:14–19
Stavenga DG, Kruizinga R, Leertouwer HL (1990) Dioptrics of the facet lenses of male blowflies *Calliphora* and *Chrysomia*. J Comp Physiol A 166:365–371
Stavenga DG, Leertouwer HL, Smits RP (1996) Light-dependent pigment migration in blowfly photoreceptors studied by in vivo CLSM. J Photochem Photobiol B 35:53–58
Warrant EJ, McIntyre PD (1993) Arthropod eye design and the physical limits to spatial resolving power. Prog Neurobiol 40:413–461
Yariv A (1985) Optical electronics. Saunders, New York